Journal of Materials Chemistry B

Accepted Manuscript

ROYAL SOCIETY OF CHEMISTRY

www.rsc.org/materialsB

Cite this: DOI: 10.1039/c0xx00000x

www.rsc.org/xxxxxx

ARTICLE TYPE

A dual-delivery system of pH-responsive chitosan-functionalized mesoporous silica nanoparticles bearing BMP-2 and dexamethasone for enhanced bone regeneration

Qi Gan,[a,b,c] Jiaoyang Zhu,[a,b] Yuan Yuan,*[a,b] Honglai Liu,[c] Jiangchao Qian,[a] Yongsheng Li,[b] Changsheng Liu*[a,b]

Received (in XXX, XXX) Xth XXXXXXXXX 20XX, Accepted Xth XXXXXXXXX 20XX
DOI: 10.1039/b000000x

Bone morphogenetic protein-2 (BMP-2) is considered as one of the most effective and extensively used growth factor to induce osteoblast differentiation and accelerate bone regeneration. Dexamethasone (Dex) with suitable dosage can enhance the BMP-2-induced osteoblast differentiation. To strengthen this synergistic osteoinductive effect, a pH-responsive chitosan-functionalized mesoporous silica nanoparticles (chi-MSNs) ensemble was fabricated for dual-delivery of BMP-2 and Dex. The MSNs are prepared by a CTAB-templated sol-gel method, and further coated by chitosan via the crosslinking of glycidoxypropyltrimethoxysilane (GPTMS). The small Dex is encapsulated in the mesopores and the large BMP-2 is incorporated into the chitosan coating. These chi-MSNs can quickly release BMP-2 in a bioactive form and then can be efficiently endocytosed and further realize a controlled release of Dex with the decreased pH value into/in cells. With the synergistic action of BMP-2 and Dex outside and inside the cell, this dual hybrid delivery system can significantly stimulate osteoblast differentiation and bone regeneration i*n vitro* and *in vivo*. Together, this dual-delivery strategy for osteogenic protein delivery may enhance clinical outcomes by retaining the bioactivity and optimizing the release mode of the drug/protein.

1. Introduction

Diseases involving bone defects and bone loss are a major clinical and public health problem, especially in elderly population. Regulation of bone formation and turnover is a complex process involving many paracrine, endocrine, and autocrine growth factors.[1, 2] Bone morphogenetic protein-2 (BMP-2), a member of the transforming growth factor beta (TGF-β) superfamily of proteins, is considered as one of the most notable cytokines with the ability to induce osteoblast differentiation and enhance bone formation and regeneration.[3-5] Dexamethasone (Dex), one of the earliest known and most readily available glucocorticoids, is proven to be an effective stimulator to enhance the BMP-2-induced osteoblast differentiation.[6, 7] This synergistic effect of BMP-2 and Dex are greatly dependent on the cell line and the dosage of Dex. For example, BMP-2 and appropriate dosage of Dex could cooperatively increase alkaline phosphatase levels in mouse C3H10T1/2 pluripotent stem cells[8] and modulate osteoblast differentiation in bone mesenchymal stem cells (bMSCs).[9]

Presenting BMP-2 in a surface-associated fashion can better mimic the native physiology and potentially enhance its effective delivery and biological effects.[10, 11] Substantial investigations have confirmed that BMP-2 requires combination with a biomaterial matrix to attain maximal efficacy. Meanwhile, as a member of TGF-β, BMP-2 first binds to the specific BMP membrane receptors, and then initiates the downstream signal transduction pathways inside cells [5]. That is to say, an ideal matrix for BMP-2 could not only promote efficient non-covalent immobilization, but also encourage proper presentation of the receptor-binding portion to the surface of the targeted cells. As another stimulator, Dex induces osteoblast differentiation in typical time- and concentration-dependent manners.[6] More importantly, Dex exerts its osteoactivity *via* binding to the glucocorticoid receptor within the cellular cytosol.[12] Therefore, to promote osteoblast differentiation efficacy, Dex must be transported intracellularly and then release in a controlled manner. Several researchers have, in fact, developed carriers to facilitate the cellular uptake of Dex.[13, 14] However, the "premature release" often limits the efficacy and undesirably increases the dosage of Dex. Inspired by the above, we hypothesize that a dual-delivery system, which can bind BMP-2 in a bioactive form and dissociate it to bind with the specific cellular receptors at the injured site, and simultaneously transport Dex into the cell and further release it in the cytosol, should be a more favorable platform to potentiate the synergistic effect of BMP-2 and Dex.

Currently, co-load and co-delivery two or more agents, such as genes, proteins or therapeutic drugs, with complementary or synergistic effect are attracting tremendously interests in nanomedicine to achieve combined therapy.[15] The key for such

therapy is to design dual delivery system that can deliver drugs to desirable sites or control the release behavior of varied drugs independently. Due to the uniform and tunable pore structure, versatility in surface functionalization, and better cellular membrane-penetrating capacity, mesoporous silica nanoparticles (MSNs), especially within the 100 - 200 nm range, have been widely used as advanced nanocarriers for intracellular delivery.[16-19] In particular, with the unique parallel pores and openings, MSNs-based stimuli-responsive "zero-order release" and controlled release systems have been developed.[20, 21] Chitosan, with a strong response in near-neutral or slightly acidic pH ranges, can be utilized as a good candidate for pH-responsive MSNs-based drug delivery.[22-26] Meanwhile, the "NH_2-" of the chitosan and the BMP-2 can form a hydrogen bond to achieve non-covalent immobilization of BMP-2. Furthermore, this polysaccharide can stimulate osteoconductivity and enhance mineralization.[27, 28] Therefore, we hypothesize that a chitosan-nanogated MSNs may be a promising nanocarrier for targeted delivery and combined therapy of BMP-2 and Dex.

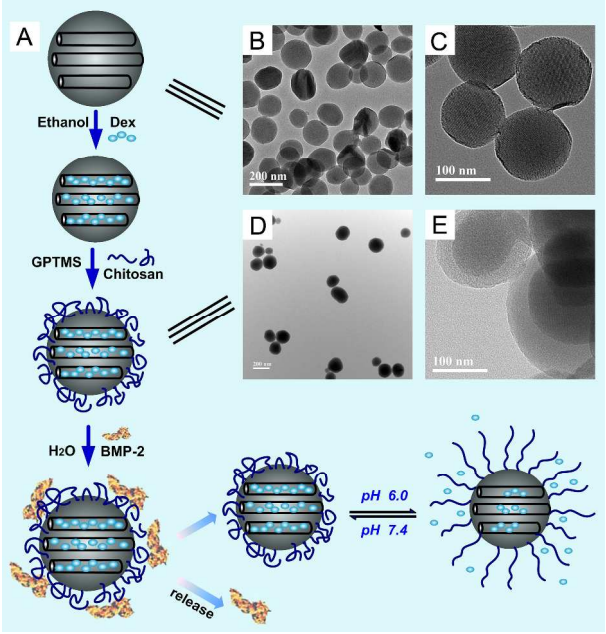

Fig. 1 (A) Schematic of synthesis of Dex/BMP-2@chi-MSNs and controlled release of BMP-2 and dexamethasone (Dex) from Dex/BMP-2@chi-MSNs; (B) TEM and (C) High resolution transmission electron microscopy (HRTEM) images of MSNs; (D) TEM and (E) HRTEM images of chi-MSNs. Scale bar = 200 nm in the TEM images of MSNs and chi-MSNs; scale bar = 100 nm in the HRTEM images of MSNs and chi-MSNs.

Based on the above rationale, in this work, a BMP-2- and Dex-loaded chitosan-functionalized MSNs (Dex/BMP-2@chi-MSNs) was fabricated to enhance bone regeneration. We first took advantage of the hydrophobic nanochannel of the MSNs to load sparingly soluble Dex. And then, the hydrophilic chitosan was coated onto the MSNs surface followed by the adsorption of BMP-2 molecule (as depicted in Fig. 1A). In this ensemble, chitosan capped onto the outlet of the MSNs was not only as a matrix to immobilize BMP-2, but also as a "gate-like" ensemble via the cross-linking of glycidoxypropyltrimethoxysilane (GPTMS) to achieve pH-responsive release of entrapped Dex within the cell. Under physiological conditions, BMP-2 was quickly dissociated from the surface of chi-MSNs, while Dex was still entrapped in the channels because of the coverage of chitosan at the pore ends. After being endocytosed into cells, with the decreasing of the pH value and the changing of dispersing states of the chitosan, the encapsulated Dex was then released into the cytosol. Consequently, BMP-2 and Dex exerted osteoblast differentiation effects outside and inside the cell simultaneously. Using rat bone mesenchymal stem cells (bMSCs) as the model cell line, we investigated the intracellular release of drugs, and the synergistic combination efficacy of Dex/BMP-2@chi-MSNs. We also investigated the *in vivo* osteoinductive effect and bone regeneration efficacy of Dex/BMP-2@chi-MSNs in a mouse hind limb muscle pocket model by using micro-computed tomographic (μCT) imaging and histological analysis. For comparison, BMP-2, BMP-2+Dex, and BMP-2+Dex loaded with MSNs (Dex/BMP-2@MSNs) were prepared and assessed.

2. Materials and methods

2.1 Materials

Fluorescein isothiocyanate isomer I, glycidoxypropyltrimethoxysilane (GPTMS), dexamethasone (Dex) and 3-(4,5-dimethylthiazol-2-yl)-2,5 -diphenyltetrazolium bromide (MTT) were all purchased from Sigma-Aldrich (CA, America). Cetyltrimethyl ammonium bromide (CTAB) and tetraethyl orthosilicate (TEOS) were from Shanghai Lingfeng Chemical Reagent Co. Ltd. (Shanghai, China). Chitosan was purchased from Shanghai Kabo Reagent Co. Ltd. (Shanghai, China). Ammonium hydroxide was from Sinopharm Chemical Reagent Co. Ltd. (Shanghai, China), and dimethyl formamide (DMF) was from Shanghai Chemical Reagent Co. Ltd. (Shanghai, China). DAPI was purchased from Beyotime Biotech Co. Ltd. (Jiangsu, China). All cell-culture related reagents were purchased from Gibco (Grand Island, NY).

2.2 Preparation of mesoporous silica nanoparticles (MSNs)

Mesoporous silica nanoparticles were prepared by a typical CTAB-templated sol-gel method[29] with minor modification. The pH value of 500 mL deionized water was adjusted to approximately 11 with 26.4 mL ammonium hydroxide (29 wt% NH_3 in water). The temperature was raised to 50 ^oC, and then 0.56 g CTAB and subsequent 2.9 mL TEOS were added with rapidly stirring. After 2 h, the sample was centrifuged and washed twice with distilled water and ethanol. The CTAB template was removed by successive thermal degradation treatments at 550 ^oC under atmospheric air for 4 h, after which the sample was allowed to slowly cool to room temperature.

2.3 Preparation of chitosan modified mesoporous silica nanoparticles (chi-MSNs)

The synthetic procedure to produce the chitosan modified mesoporous silica nanoparticles is showed as following steps. 0.5 g of chitosan (average molecular weight of 3.0×10^4 $g \cdot mol^{-1}$, 90% deacetylation) was dissolved in 50 mL of aqueous 2% acetic acid solution (HAc) under strongly magnetic stirring to obtain a sticky solution. 0.5 mL aliquot of 20% GPTMS in ethanol solution was added into 20 mL aliquot of the 1% chitosan solution (referred to as 1:40 GPTMS/chitosan in this study). The solution was mixed in a sealed plastic bottle and then allowed to

stay at room temperature for at least 24 h. 0.25 g MSNs were dispersed in 25 mL of chitosan/GPTMS solution and then stirred at room temperature for at least 8 h. the as-synthesized solid was filtered, washed with deionized water, and then dried under vacuum to get chi-MSNs.

2.4 Characterization

The FTIR spectrum was measured by ATR on Nicolet 380 (Thermo, USA). X-ray diffraction patterns were obtained in a RINT2000 vertical goniometer (Rigaku, Japan) using Cu Kα irradiation. Surface analysis of the materials was performed by nitrogen sorption isotherms in a Micromeritics ASAP2010 sorptometer (Micromeritics, USA). The surface areas were calculated by the Brunauer-Emmett-Teller (BET) and the pore size distributions were obtained by the Barrett-Joyner-Halenda method. TEM and high-resolution TEM (HRTEM) were performed on a transmission electron microscope (JEM-2100, Japan) with a field emission gun operating at 200 KV. The zeta potential and hydrodynamic radius of the nanoparticles were studied with a particle size analyzer Malvern Nano HT Zetasizer (Malvern, UK). UV-visible spectroscopy was carried out with a UV/Vis spectrometer (Sunnyvale, CA).

2.5 Drug loading into/onto chi-MSNs

0.25 g MSNs was dispersed in 5 mL anhydrous ethanol and then 50 mg Dex was added. The suspension was sonicated for 5 minute and kept in a shaker at room temperature. After 4 h impregnation, 25 mL of chitosan/GPTMS solution was added into the above solution and the reaction was continued at room temperature for another 8 h. Dex-entrapped chi-MSNs were filtered and washed twice with deionized water, and then dried under vacuum to obtain Dex@chi-MSNs. The loading of Dex by MSNs and chi-MSNs are 29 mg/g and 35 mg/g, respectively. FITC-entrapped chi-MSNs nanoparticles (FITC@chi-MSNs) were prepared by the same method.

To prepare Dex/BMP-2@chi-MSNs, a certain amount of Dex@chi-MSNs was further redistributed in BMP-2 solution (E. coli-derived, Rebone, Shanghai, China) (50 μg/mL) and stayed for 4 h. Then the solution was filtered and the BMP-2-loaded nanoparticles (Dex/BMP-2@chi-MSNs) were freeze dried and stored at 4 ^{o}C for later use.

Dex/BMP-2@MSNs was prepared by similar steps. 0.25 g MSNs was dispersed in 5 mL anhydrous ethanol and then 50 mg Dex was added. The suspension was sonicated for 5 minute and kept in a shaker bath for 4 h at room temperature. Then the solid was filtered and washed twice with deionized water, and then dried under vacuum to obtain Dex@MSNs. The subsequent steps were similar to the fabrication of Dex/BMP-2@chi-MSNs. BMP-2@chi-MSNs was fabricated as followed: a certain amount of chi-MSNs was distributed in BMP-2 solution (50 μg/mL) and stayed for 4 h to absorb the BMP-2. Then the solution was centrifuged and the nanoparticles were collected. Finally the precipitated nanoparticles were lyophilized and weighted until use. The loading of BMP-2 by MSNs and chi-MSNs are 120 μg/g and 248 μg/g, respectively.

2.6 *In vitro* Dex and BMP-2 release

100 mL PBS with various pH values were used for evaluating the Dex release from the pore voids of the chitosan-functionalized materials (Dex@chi-MSNs and Dex/BMP-2@chi-MSNs). For example, a dialysis bag loaded with 20 mg Dex@chi-MSNs (or Dex/BMP-2@chi-MSNs) was placed into a ZTY Auto Temperature sink (Jiangsu, China) filled with PBS solutions at a certain pH. The system was then maintained in circulation and at 37 ^{o}C for 80 min. The release of Dex from the pore voids to the PBS was monitored via UV-Vis spectrum measurement with the band of the drug centered at 242 nm.

To investigate the *in vitro* release profiles of BMP-2 from chi-MSNs and MSNs, the BMP-2@chi-MSNs, Dex/BMP-2@chi-MSNs and BMP-2@MSNs nanoparticles were separately put into a centrifuge tube containing 1 mL PBS solution (pH = 6.0/7.4). The tubes were incubated at 37 ^{o}C for 24 h. At the end of each time point, the suspension was centrifuged and 0.5 mL of the release medium was collected. Then 0.5 mL fresh PBS solution (pH = 6.0/7.4) was added into it immediately. Because a certain amount of protein was extracted from the release fluid and could not be reflected in the later sampling point, a corrected method[30] was used to calculate the actual amount of BMP-2 release from carrier materials. BMP-2 concentration was determined using a BMP-2 ELISA kit (PeproTech, Rocky Hill, NJ).

2.7 Cell culture

Rat bMSCs were flushed out of the femora and tibias of rats with Dulbecco's modified Eagle's medium-low glucose (DMEM-LG, Gibco) by a 5-mL syringe. The cells were seeded in 37.5 cm^2 flasks containing MEME-LG supplemented with 10% fetal bovine serum in a humidified atmosphere with 5% CO_2 at 37 ^{o}C, and the medium was changed every 3 days. When reached 80% confluency in the flasks, the cells were trypsinized with 0.25% trypsin/0.03% ethylene diamine tetraacetic acid (EDTA) and expanded into a plate as passage 1. All assays were performed on second passage cells after enlarged cultivation.

2.7.1 Cytotoxicity assay

The cytotoxicity of MSNs and chi-MSNs was evaluated with an MTT assay. The bMSCs were plated into 24-well plates at a density of 1.5 × 10^4 cells/well in 1.0 mL culture medium and incubated for 24 h. Afterwards, the culture medium was removed and the cells were washed with PBS twice, then each well was added with 1.0 mL medium with different particles at different concentrations of 50, 100 and 200 μg/mL. The MTT assay was performed following the standard protocol after incubating cells for 1, 3 and 5 days.

2.7.2 Determination of alkaline phosphatase (ALP) activity

The bMSCs were seeded into 24-well plates at 5 × 10^4 cells/well in DMEM-LG. After 24 h cell adhesion, the culture medium was replaced with 1.0 mL DMEM-LG containing different concentrations of synthesized nanoparticles. At day 7, 14 and 21, the culture medium in wells was aspirated. Then about 200 μL of 1% Nonidet P-40 (NP-40) was added into each well at room temperature and incubated for 1 h. 50 μL of the obtained cell lysate was added to 96-well plates, 50 μL of 2 mg/mL p-nitrophenylphosphate (Sangon, Shanghai, China) substrate solution composed of 1 mmol/L $MgCl_2 \cdot 6H_2O$ and 0.1 mol/L glycine was added. Then it was incubated at 37 ^{o}C for 60 min. The reaction was quenched by 100 μL of 0.1 N NaOH, and the ALP value was quantified at a wavelength of 405 nm using a

microplate reader (SPECTRAmax 384, USA). ALP activity was expressed as 405 nm O.D. value per min per mg of total protein. Protein concentration was determined using the BCA Assay Kits (Beyotime, Jiangsu, China), with bovine serum albumin as the standard.

2.7.3 Measurement of mineralization

A mineralized extracellular matrix was stained with Alizarin red S to determine the bone mineralization. The bMSCs were plated in 24-well plates at 1.0×10^4 cells/well and adhered for 24 h. After that, the culture medium was replaced with 1.0 mL DMEM containing different concentrations of inducers or materials containing inducers. The cells were cultured for 14 and 21 days, and the culture medium was replaced every 3 days. At the end of incubation, cells were washed with PBS and fixed with cold 1% glutaraldehyde (w/v) in PBS for 10 min. Fix cells were stained with 1% Alizarin Red (Major Biotech, SH, China) for 10 min. Then the cells were rinsed with ultrapure water and the mineralization pictures were captured with inverted light microscope.

2.7.4 Real-time reverse transcription polymerase chain reaction (real-time RT-PCR) analysis

The bMSCs were seeded in 6-well plates at 8×10^4 cells/well in DMEM-LG. Then the cells were cultured with DMEM-LG in the presence of different inducers. At 4 and 7 days, the total cellular RNA was extracted using Trizol reagent (Takara, Tokyo, Japan) according to the manufacturer's instructions. First-stranded cDNA was synthesized with PrimeScript RT reagent Kit (Takara, Tokyo, Japan). Subsequently, cDNA was diluted ten-fold in sterile distilled water and 4 μL aliquot of the diluted cDNA was subjected to real-time RT-PCR using SYBR Premix Ex Taq™ (Takara, Tokyo, Japan). Real-time RT-PCR was performed in a 10 μL solution containing 1 × PCR buffer, 4 μL aliquot of the diluted cDNA, 1 × SYBR Premix Ex Taq (5 μL), 0.2 μM (0.4 μL) of each primer (forward and reverse), and 0.2 μL ROX Reference Dye (50×). The conditions of real-time PCR were as follows: 95 °C for 30 sec followed by 40 cycles at 95 °C for 5 sec and 60 °C for 34 sec. Real-time PCR was performed by a Bio-Rad real-time PCR system (Bio-Rad, Hercules, CA, USA) on markers of ALP, runt-related transcription factor 2 (Runx2), collagen I (Col I), osteocalcin (OCN) and osteopontin (OPN). The forward and reverse primer sequences used in this study are listed in Table S1.

2.8 Enhanced cellular uptake of drugs in the presence of chi-MSNs

Dex is a kind of hydrophobic glucocorticoid and used clinically as an anti-inflammatory agent. In order to track the cellular uptake of drugs, a hydrophobic green dye, Fluorescein isothiocyanate isomer I (FITC), was selected as a model drug.

2.8.1 Cellular uptake of FITC

bMSCs were plated at a density of 3×10^4 cells/well on chamber slides with DMEM-LG. After 24 h, the medium was supplemented with free FITC, FITC loaded with chi-MSNs (FITC@chi-MSNs). The loading efficiency of FITC was nearly 14% and the concentration of the FITC entrapped hybrid materials added to the cells was 100 μg/mL as the same as the concentration of free FITC. After 4 h incubation, the cells were washed with PBS (pH = 7.4) twice, then re-incubated for 30 minutes in PBS containing 3.7% formaldehyde and followed with 57.0 mM DAPI. After incubation, the solution was removed and the slides were covered with 50% glycerol in water. The DAPI-stained nuclei and FITC were monitored with CLSM (Nikon, Japan).

2.8.2 Flow cytometry analysis

bMSCs were plated at a density of 2.0×10^5 cells per well in 35 mm Corning dishes and incubated for 24 h. After attachment, the cells were cultured with medium containing free FITC or FITC@chi-MSNs, respectively. The concentrations of FITC and FITC@chi-MSNs were similar to the cellular uptake experiment. After 4 h incubation, these cells were washed with PBS (2×) and then harvested by trypsinization. The cells were centrifuged, rinsed with PBS and resuspended in PBS at a concentration of 1.0×10^6 cells/mL. Then the cells were immediately analyed with a flow cytometer at an emission wavelength of 530 nm for FITC.

2.9 Exploration of the mechanism of BMP-2@chi-MSNs-induced enhanced osteogenic differentiation *in vitro*

The conformation and bioactivity of the free BMP-2, BMP-2 released from MSNs at pH 6.0 and 7.4, BMP-2 released from chi-MSNs at pH 6.0 and 7.4 were investigated to explore the BMP-2@chi-MSNs-induced excellent osteogenic differentiation. The concentration of BMP-2 for test was 2 μg/mL in each group. The Far-UV circular dichroism (CD) spectrum is an effective method for investigating the secondary structure of proteins.[31] In our study, we used CD analysis to detect the changes of the secondary structure and conformation of BMP-2. The free BMP-2, BMP-2 released from MSNs at pH 6.0 and 7.4, BMP-2 released from chi-MSNs at pH 6.0 and 7.4 were analyzed at 25 °C in a 1.0 mm path length quartz cell with a time constant of 0.25 s and a scan rate of 100 nm/min using a spectropolarimeter (Model J-715, Tokyo, Japan). The bandwidth was 1.0 nm and 5 scans were accumulated. The effect of loaded materials and pH on BMP-2-induced ALP activity was also studied. The bMSCs were cultured in 24-well plates for 24 h. After attachment, the cells were separately cultured with medium containing free BMP-2, BMP-2 released from MSNs at pH 6.0 and 7.4, BMP-2 released from chi-MSNs at pH 6.0 and 7.4. At day 7, 14 and 21, the ALP activity was determined. To determine the ALP activity histochemically, after 7-days-cultivation, cells were fixed with 1% glutaraldehyde for 10 min on ice, washed with PBS, and incubated with 0.5 mL BCIP/NBT Alkaline Phosphatase Color Development Kit (Beyotime, Jiangsu, China) for 30 min at 37 °C. Stained cells were imaged with TE-2000U inverted light microscope (Nikon, Japan).

2.10 Ectopic bone formation *in vivo*

The animal experiment adhered to the NIH guidelines for the care and use of laboratory animals (NIH Publication No. 85-23 Rev. 1985) and was approved by the Research Center for Laboratory Animal of Shanghai University of Traditional Chinese Medicine. Four implants groups were prepared: (1) Gelfoam loaded with 15 μg of BMP-2 (BMP-2); (2) Gelfoam loaded with 15 μg of BMP-2 and 20 μg of Dex (BMP-2+Dex); (3) Gelfoam loaded with MSNs containing 15 μg of BMP-2 and

20 μg of Dex (Dex/BMP-2@MSNs); (4) Gelfoam loaded with chi-MSNs containing 15 μg of BMP-2 and 20 μg of Dex (Dex/BMP-2@chi-MSNs). These materials were freeze dried, and stored at -20 °C until used. Forty-eight male mice (4 weeks old, Silaike Inc. Shanghai, China) were anesthetized by intraperitoneal injection of pentobarbital (0.06 g/kg). The mice were divided into 4 groups and implanted with the Gelfoam into right thigh muscle pouches. At 2 and 4 weeks after implantation, the mice were sacrificed with an overdose of pentobarbital and the implants were harvested.

2.10.1 Micro-computed tomography (μCT)

The bone formation was evaluated with μCT scan images (eXplore Locus SP, GE, USA). A voltage of 80 kV and current of 80 mA were used in all scans. Projection images were taken at 0.4° increments over 360°. Bone radiomorphometric analysis was performed by using GE Microview ABA 2.1.2 software. The 3D images were finally redigitized with a 16-bit data format, proportional to the measured attenuation coefficients of the voxels. The amount of bone formation was quantified as the bone volume and tissue mineral density within the defined VOI (volume of interest) in each defect site.

2.10.2 Histological analysis

After fixation with 4% neutral buffered formalin for 48 h, the ectopic bone samples were decalcified in 12.5% EDTA, dehydrated in a graded series of alcohol, and embedded in paraffin. Serial 10-μm thick sections from each group were stained with hematoxylin/eosin (HE) after decalcification and observed microscopically.

2.11 Statistical analysis

All numerical data were expressed as the mean ± standard deviation. Statistical analysis was performed with one-way analysis of variance (ANOVA). A value of $p < 0.05$ was considered as statistical significance.

3. Results and Discussion

3.1 Design and synthesis of chi-MSNs

In order to develop a pH-responsive chi-MSNs delivery system, mesoporous MCM-41 nanoparticles of about 100 - 200 nm diameter were prepared and further coated with chitosan *via* the cross-linking of GPTMS (Fig. S1). Our data are in full agreement with this notion. The physicochemical properties of the MSNs and chi-MSNs were compared. The morphologies and microstructures of the prepared MSNs and chi-MSNs were clearly revealed by TEM. As shown in Fig. 1B, the mesoporous nanoparticles were uniform spherical nanoparticles with a mean diameter of approximately 130 nm. In addition, the streak structural features and highly ordered mesoporous network with a hexagonal array could be clearly observed from the HRTEM image of the synthesized nanoparticles (Fig. 1C), which was a characteristic feature of MCM-41-type MSNs. After functionalized with chitosan, the nanoparticles were found to have a typical core-shell structure, and the typical mesoporous channels (with alternate black and white stripes) could be found in the HRTEM images of chi-MSNs (Fig. 1E). The chi-MSNs showed much better dispersibility (Fig. 1D and Fig. 2A). The FTIR spectra for both MSNs and chi-MSNs displayed transmission peaks at about 1084 cm^{-1}, 803 cm^{-1}, and 462 cm^{-1}, which were assigned to the characteristic stretching vibrations of the Si-O bond (Fig. 2B).[32] In addition, the increased specific band of chi-MSNs could be attributable to the vibration of C-H bond.[33]

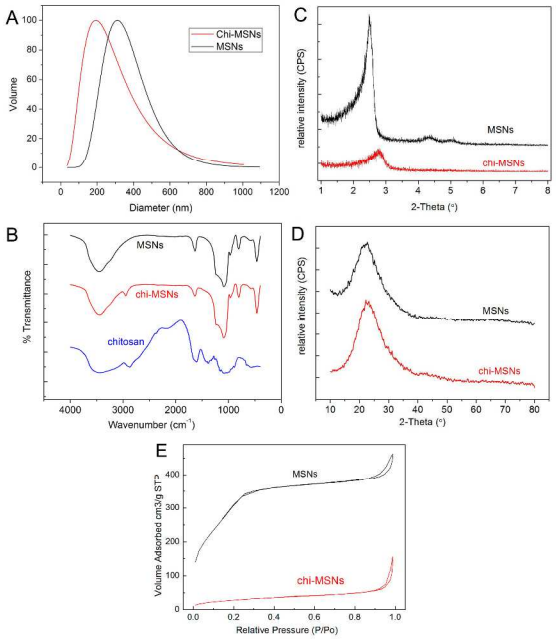

Fig. 2 Characterization of as-prepared MSNs and chi-MSNs. (A) The dynamic light scattering (DLS) results of both materials, (B) FTIR spectra of MSNs, chitosan and chi-MSNs. (C) Small-angle powder XRD of MSNs and chi-MSNs from 2θ = 1-8°. (D) Wide-angle powder XRD of MSNs and chi-MSNs from 2θ = 10-80°. (E) Nitrogen adsorption/desorption isotherms of MSNs and chi-MSNs.

The ordered mesoporous structure was confirmed by small-angle XRD measurements (Fig. 2C). In this figure, the prepared MSNs exhibited a typical MCM-41-type structure[34] with three well-resolved diffraction peaks assigned as (100), (110), and (200) reflections. After modified with chitosan, a relatively weak peak of 2.80° could be found in the diffraction patterns, with the concomitant loss of the (110) and (200) reflections. Fig. 2D revealed that the chitosan-modified and unmodified MSNs both are amorphous structure. In the liquid nitrogen isotherms (Fig. 2E), the unmodified MSNs exhibited a type IV isotherm by IUPAC classification.[34] However, after coated with chitosan, the N_2 sorption isotherms of chi-MSNs showed a relatively flat isotherm, accompanied by a loss of hysteresis loop. After being modified, the surface area of chi-MSNs calculated by the Barrett-Joyner-Halenda (BJH) method decreased from 960.7 $m^2 \cdot g^{-1}$ of MSNs to 131.8 $m^2 \cdot g^{-1}$ (Table 1), and the pore volume also decreased from 0.98 $cm^3 \cdot g^{-1}$ to 0.16 $cm^3 \cdot g^{-1}$. The pore size decreased to almost zero, which means the pores were completely blocked by chitosan wrapping. The increase of zeta potential from -22.3 mV to +22.5 mV also confirmed the successful functionalization of MSNs by chitosan. From the results of TGA (Fig. S2), the chitosan content in chi-MSNs is about 35%.

Table 1. Nitrogen adsorption/desorption isotherms and ζ-potential measurement data of MSNs and chi-MSNs samples.

Sample	BET surface area (m^2/g)	Pore volume (cm^3/g)	Pore size (nm)	ζ-potentials (mV)
MSNs	960.7	0.98	2.7	-22.3
chi-MSNs	131.8	0.16	-	+22.5

3.2 Cellular response to the MSNs and chi-MSNs

In order to explore the biocompatibility and feasibility of the dual delivery carrier, cell proliferation and differentiation of the MSNs and chi-MSNs were first investigated in bMSCs. According to the MTT measurement (Fig. S3A), cell proliferation was significantly increased after incubated with chi-MSNs compared to that with MSNs at each time point. Furthermore, by determining the typical marker of osteoblast differentiation of ALP activity, it was demonstrated that the ALP activities of the chi-MSNs groups greatly improved with the increase of the concentration of chi-MSNs. Specifically, from Fig. S3B, the group with 200 μg/mL chi-MSNs showed the highest ALP activity at day 21. The results suggest that the chi-MSNs facilitate the proliferation of bMSCs and differentiation of bMSCs to osteoblasts. According to the previous studies, this good long-term biocompatibility and enhanced *in vitro* osteoinductivity of chi-MSNs may be related to the natural properties of chitosan.[23, 26]

3.3 Release and bioactivity of the BMP-2 from chi-MSNs

Highly efficient delivery and preservation of the bioactivity of BMP-2 are extremely crucial for appropriate use of BMP-2.[31, 35] The *in vitro* release kinetics of BMP-2 was studied by immersing the BMP-2-loaded MSNs and chi-MSNs into the PBS solution. As shown in Fig. 3A and Fig. S5, BMP-2 from MSNs or chi-MSNs all exhibited a quick 'initial burst' release followed a relative slow release. In contrast, in the initial 6 h, the release of BMP-2 from MSNs (about 60% ~70% release) was obviously slower than that from the chi-MSNs (over 80%), but after 6 h release, similar slopes/release rates were observed on all groups.

We think this slight difference of BMP-2 release from varied MSNs-based nanocarriers results from the different functional groups on the mesopore surface and their diverse electrostatic interactions with BMP-2. BMP-2 is a positively charged protein at pH of 6.0 or 7.4. But the zeta potentials of MSNs and chi-MSNs are -22.3 and +22.5 mV. In the BMP-2-induced osteogenesis process, the initial protein burst release after implantation is preferable to achieve a fast start up of osteogenesis, and the sustainably released protein is necessary to maintain a local BMP-2 concentration for a sufficient period.

Compared the release of BMP-2 from chi-MSNs with and without Dex, it can be seen that Dex have little effect on the release behavior of BMP-2 from the chi-MSNs. Our previous investigation reported that the cellular uptake of MSNs nanoparticles with about 100 - 200 nm mainly occurred in the initial 4 h.[36] Therefore, before entered into the cytoplasm, most BMP-2 was released into the surrounding environment.

To test the bioactivity of BMP-2 released from MSNs and chi-MSNs, ALP expression was measured quantitatively. From Fig. 3B, it could be seen that the bMSCs treated with BMP-2 released from chi-MSNs showed higher ALP activity than the cells treated with BMP-2 from MSNs. At the specific time point, the ALP activity of BMP-2 released from chi-MSNs at pH 6.0 was similar to that released at pH 7.4, indicating that pH was not the main factor influencing the ALP activity of BMP-2 in this experiment. The histochemical analysis (Fig. 3C) stained with the BCIP/NBT ALP Color Development Kit also revealed that cells treated with BMP-2 released from chi-MSNs both at pH 6.0 and pH 7.4 exhibited high ALP activity, which proved that chi-MSNs was an effective carrier of BMP-2.

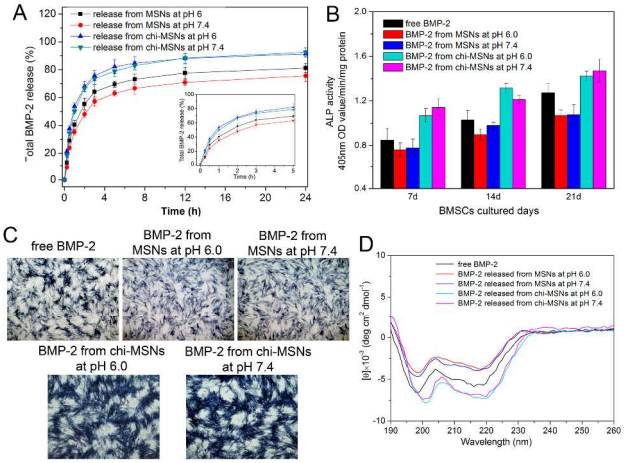

Fig. 3 In vitro release profiles and bioactivity of BMP-2 from MSNs-based carriers. (A) Cumulative release of BMP-2 in phosphate buffer solution (PBS) at pH 6.0 and 7.4. (B) Alkaline phosphatase (ALP) activity of BMP-2 released from different carriers. bMSCs were cultured for 7, 14 and 21 days with free BMP-2, BMP-2 released from MSNs, and BMP-2 released from chi-MSNs at pH 6.0 and 7.4. (C) ALP activity was histochemically detected using BCIP/NBT Alkaline Phosphatase Color Development Kit after culture for 7 days. (D) Far-UV CD spectra of free BMP-2 and BMP-2 released from MSNs and chi-MSNs at pH 6.0 and 7.4.

To further explore the differences in bioactivity between BMP-2 released from various carriers, the conformations and secondary structures of BMP-2, BMP-2 released from MSNs, and BMP-2 released from chi-MSNs at pH 7.4 and 6.0 were measured by circular dichroism (CD) spectroscopy (Fig. 3D). The free BMP-2 in PBS manifested an intense positive peak at 195 nm and two minus peaks at 208 nm and 220 nm corresponding to α-helix of BMP-2. BMP-2 released from chi-MSNs at pH 7.4/6.0 showed slightly enhanced minus peaks, which suggest an increased α-helix of BMP-2. In contrast, for the BMP-2 released from MSNs, the two minus peaks were weakened, indicating reduction of the α-helix. The secondary structure compositions of BMP-2 released from MSNs and chi-MSNs at pH 7.4/6.0 in PBS were determined (Table S2). After being absorbed and released from MSNs, compared with the free BMP-2, the percentages of the α-helix and β-sheets/β-turns of BMP-2 decreased at both pH 6.0 and pH 7.4. However, the α-helix of BMP-2 released from chi-MSNs increased to 15.4% at pH 6.0 and 15.7% at pH 7.4. The changes in the folding structure of BMP-2 from MSNs were all bigger than those from chi-MSNs at pH 6.0 and pH 7.4. Previous studies have demonstrated that hydrophobic interactions between a polypeptide/protein and an inorganic surface might result in deactivation of the polypeptide/protein due to the collapse of its secondary or tertiary structure.[37, 38] Therefore, from this

viewpoint, the desirable conformation and bioactivity of BMP-2 might be related to the hydrophilic surface of the chitosan.

3.4 Controlled release and intracellular uptake of Dex

Considering the fact that the targeted receptor of Dex resides within the cytosol of the cell, the "zero-order release" in the delivery process and subsequent pH-triggered release after cellular uptake by cells are expected for the carrier. In this experiment, pH-responsive regulation efficiency of these hybrid materials was investigated using two kinds of PBS solutions at different pH values. As shown in Fig. 4A, when the pH value of PBS was 6.0, Dex was released almost immediately from the chitosan-modified MSNs. In particular, nearly 85% Dex was released within 60 min. However, almost no drug release from chi-MSNs was detected when the pH value of PBS was raised to 7.4, which confirmed absence of leakage of the entrapped drug and a good coating efficiency of the chitosan. We can also found that Dex released from Dex@chi-MSNs and Dex/BMP-2@chi-MSNs exhibited a similar release behavior (Fig. S6).

Furthermore, changes in release behavior with changes in pH are shown in Fig. 4B. In the initial 30 min, there was no drug released when the pH of the release medium was 7.4. When the pH was suddenly changed to 6.0 with 1 M HCl at 30 min, significant release of Dex was detected. After 10 min, the pH was set back to 7.4 and as a result, the release of Dex significantly decreased. The repeatability of the experiment was verified by a second switching, and a similar result was observed. What is more, Dex release profile from unmodified MSNs (Fig. S7) has demonstrated that the pH-sensitive released of Dex was due to the gating effect of chitosan.

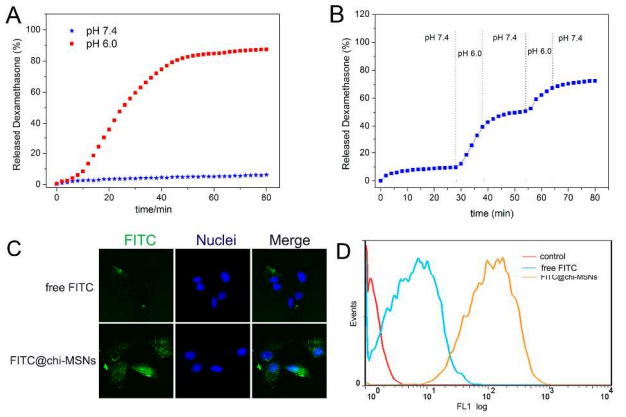

Fig. 4 *In vitro* release curves and intracellular uptake of Dex. (A) Release of Dex from chi-MSNs at pH 6.0 and 7.4. (B) Partial Dex release from chi-MSNs as a function of pH variations. (C) Confocal microscopy images of cellular uptake of FITC in bMSCs with free FITC and FITC@chi-MSNs after 4 h. (D) Flow cytometry analysis of bMSCs incubated with free FITC and FITC@chi-MSNs after 4 h incubation.

To demonstrate the role of pH value played in the open/close of the pore of MSNs and the ensuing controlled release of Dex, the nitrogen adsorption/desorption isotherms of chi-MSNs immersed at pH 6.0 and 7.4 were measured and the results were showed in Fig. S8. The BET surface area of chi-MSNs was 152.1 $m^2 \cdot g^{-1}$ at pH 7.4 while it was increased to 547.9 $m^2 \cdot g^{-1}$ after the nanoparticles were immersed into PBS at pH 6.0 for 30 min (Table S3). It is well-accepted that the charged chitosan chains exhibit loop and tail conformations on a surface, depending on the pH value of the surrounding environment. The loop conformation can be formed by deprotonation of primary amino groups on chitosan under physiological conditions, while the tail conformation can be formed with protonation at pH below its isoelectric point.[39] Therefore, by reversible transformation of different dispersing states of chitosan at the physiological pH of body fluids (or the extracellular environment) and at acidic pH (around 6.0 and 5.0 in the intracellular early endosomes and late endosomes/lysosomes), a desirable on/off switching function can be achieved.

Next, we used fluorescein isothiocyanate isomer I (FITC, a hydrophobic green dye) as a model drug[40] to investigate the cellular uptake of drugs in the presence of chi-MSNs. From the confocal laser photographs (Fig. 4C), after 4 h exposure, it is evident of a large amount of FITC in the cell in the presence of chi-MSNs in bMSCs. The flow cytometry analysis results (Fig. 4D) also confirmed the higher fluorescent intensity of the bMSCs internalized with FITC@chi-MSNs, almost 12-fold higher than that of free FITC-internalized. These qualitative and quantitive results revealed that, as expected, the chitosan-modified MSNs could serve as efficient carriers for enhanced intracellular release of Dex.

3.5 Osteogenic differentiation and mineralization of bMSCs with Dex/BMP-2@chi-MSNs

To examine whether the synergistic osteogenic differentiation efficacy of BMP-2 and Dex could be promoted by the chi-MSNs carrier, the ALP activity and cell mineralization were detected. From Fig. 5A, it was found that after incubated with a medium containing BMP-2 and Dex, the ALP activities all increased significantly at appointed culture days in contrast with the control. For the comparison, the Dex/BMP-2@chi-MSNs group displayed much higher ALP activity than the Dex@chi-MSNs and the BMP-2@chi-MSNs. On the other hand, for the combined Dex and BMP-2 groups, the ALP activity of the Dex/BMP-2@chi-MSNs group was obviously higher than that of the Dex-BMP-2 and the Dex/BMP-2@MSNs. These results revealed the enhanced osteoblast differentiation capacity of the targeted-delivery system of Dex/BMP-2@chi-MSNs.

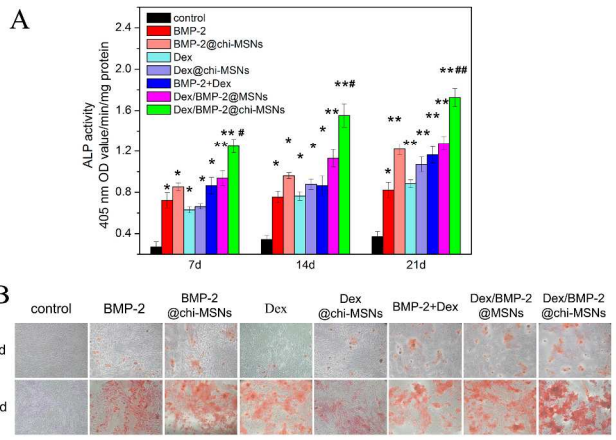

Fig. 5 Effect of BMP-2, BMP-2@chi-MSNs, Dex, Dex@chi-MSNs, BMP-2+Dex, Dex/BMP-2@MSNs and Dex/BMP-2@chi-MSNs on ALP activity for 7, 14 and 21 days (A) and mineralization (B) in bMSCs cultured at day 14 and 21. (BMP-2 is 2 μg/mL and Dex is 100 nM, *p < 0.05, **p < 0.001, compared with control; #p < 0.05, ##p <0.001, Dex/BMP-2@MSNs vs. Dex/BMP-2@chi-MSNs).

Mineralization patterns examined by Alizarin red S staining (Fig. 5B) indicated that at day 14, mineralization of all the experimental groups is not obvious. However, after 21 days incubation, cells treated with Dex/BMP-2@chi-MSNs showed greater speckled patterns, indicative of mineral nodule formation, than the other groups.

The gene expression of osteogenic transcription factors and osteoblast markers were also measured with real-time RT-PCR assay. From Fig. 6A, it was found that the mRNA expression levels of ALP were increased significantly after incubated with Dex/BMP-2@chi-MSNs. Similar to the results obtained in ALP gene expression analysis, the mRNA expression of Runx2 (Fig. 6B) and OPN (Fig. 6C), also significantly increased in bMSCs cultured with Dex/BMP-2@chi-MSNs, in contrast with those cultured with BMP-2, BMP-2 + Dex, and Dex/BMP-2@MSNs. Collagen I mRNA expression (Fig. 6D) was significantly increased by Dex/BMP-2@chi-MSNs treatment during the culture period, but the OCN mRNA expression (Fig.6E) was significantly increased by both Dex/BMP-2@chi-MSNs treatment and Dex/BMP-2@MSNs treatment.

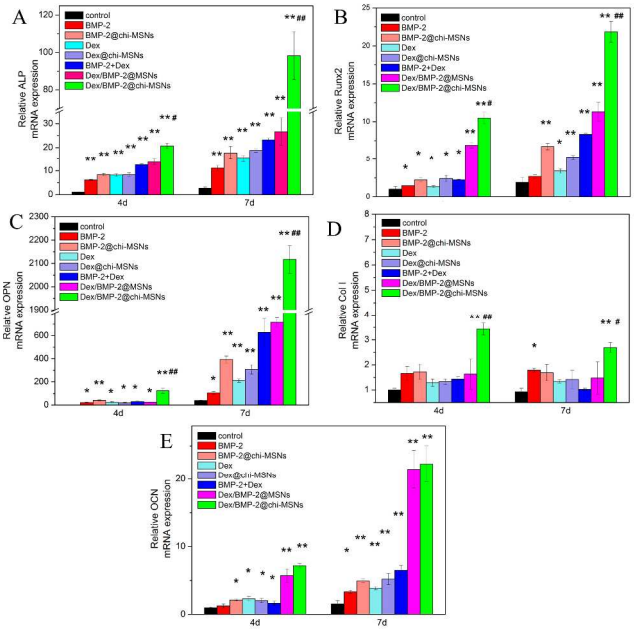

Fig. 6 Effect of BMP-2, BMP-2@chi-MSNs, Dex, Dex@chi-MSNs, BMP-2+Dex, Dex/BMP-2@MSNs and Dex/BMP-2@chi-MSNs on the expression of osteogenic marker gene ALP (A), Runx2 (B), OPN (C), Col I (D), and OCN (E) in bMSCs cultured at day 4 and 7 by real-time RT-PCR analysis. (BMP-2 is 2 μg/mL and Dex is 100 nM, *p < 0.05, **p < 0.001, compared with control; #p < 0.05, ##p <0.001, Dex/BMP-2@MSNs vs. Dex/BMP-2@chi-MSNs).

3.6 Ectopic bone formation in mice

In order to further investigate the osteogenic capacity of Dex/BMP-2@chi-MSNs *in vivo*, we evaluated ectopic bone formation in the thigh muscle pouches of mice. The digital photos (Fig. 7A) and 3D μCT restructured images (Fig. 7B) showed that there was obvious bone formation in all four groups at 2 weeks and 4 weeks. The Dex/BMP-2@chi-MSNs induced significantly more ectopic bone formation than the other groups within 2 weeks and 4 weeks. The generated bone volumes (Fig. 7C) and tissue mineral density (Fig. 7D) were also calculated to evaluate the bone formation. The results demonstrated that the Dex/BMP-2@chi-MSNs group contained the highest bone volume at both 2 weeks and 4 weeks. Compared to other groups, the bone volume of the Dex/BMP-2@chi-MSNs group increased nearly 100% at 4 weeks. Interestingly, in comparison to the findings obtained at 2 weeks, the bone volumes of BMP-2 and BMP-2+Dex groups had decreased at 4 weeks, while that of MSNs and chi-MSNs containing BMP-2 and Dex had increased at 4 weeks. Furthermore, there was no significant difference between the tissue mineral densities of the four groups at 2 weeks. However, the tissue mineral densities of Dex/BMP-2@chi-MSNs and Dex/BMP-2@MSNs were significantly higher than the other two groups at 4 weeks ($p < 0.05$).

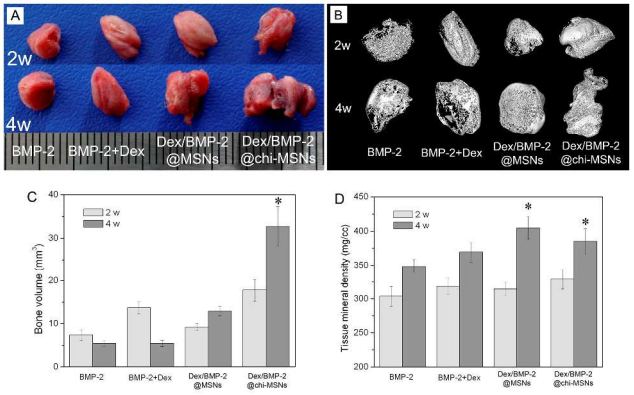

Fig. 7 Ectopic bone formation induced by BMP-2 and Dex in vivo. Digital photos (A) and 3D μCT images (B) of new bone formation with different implants after 2 and 4 weeks post-implantation. Quantitative analysis of regenerated bone volume (C) and tissue mineral density (D) from 3D μCT images was performed by using GE Microview ABA 2.1.2 software. (The dosages of BMP-2 and Dex are 15 μg and 20 μg, *p < 0.05, compared with BMP-2 group at 4 weeks).

For histological evaluations of the ectopic bone formation, histological staining with H&E was performed to compare tissue morphology and composition of the ectopic bone at 4 weeks (Fig. 8). Bone tissue that was found in all four groups indicated moderate bone formation with BMP-2. A large amount of fibrous tissue was observed only in the BMP-2-treated groups. After the ectopic osteogenesis for 4 weeks, large numbers of lipocytes in the BMP-2+Dex-treated group were observed, which was referred to as medulla ossium flava.[35] However, in the Dex/BMP-2@MSNs group, a large amount of trabecular bone as well as red bone marrow was observed, while the amount of trabecular bone was the greatest in the Dex/BMP-2@chi-MSNs group.

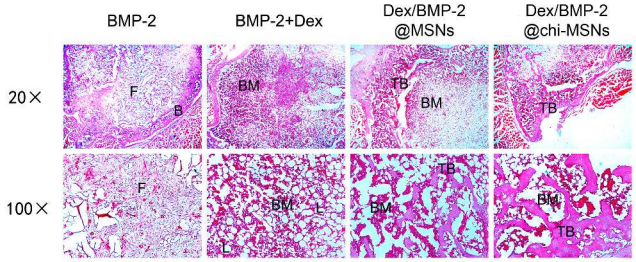

Fig. 8 Histological evaluation with H&E of ectopic bone formation at 4 weeks. (F: fibrous tissue, L: lipocytes, B: bone, TB: trabecular bone, BM: bone marrow).

Since small Dex drugs mainly locates in the mesopores and large BMP-2 are loaded into the chitosan coating, our synthesized Dex/BMP-2@chi-MSNs reveal desired release of BMP-2 and Dex outside and inside the cells. As anticipated, the above *in vitro* and *in vivo* results obtained here indicate that the dual-drug delivery system fabricated here can indeed enhance the synergistic effect of BMP-2 and Dex in osteoblast differentiation of bMSCs cells *in vitro* and trigger osteogenesis in the mouse hind limb muscle pocket model. Based on the previous investigations and the results presented here, a simple model is proposed, as illustrated in Fig. 9. Functionalization of chitosan on the outer surface not only endows nanoparticles with good dispersibility, biocompatibility, and cellular uptake, but also makes it favorable to maintain the effective bioactivity of loaded protein. Once in the physiology environment, BMP-2 is quickly released from the ensemble and binds to its specific cell surface receptors. After that, Dex is effectively taken up by cells in the presence of chi-MSNs and forms complexes, binding to its receptor in the cytosol. Consequently, BMP-2 activates downstream Smad signaling effect outside the cell and Dex initiates the osteoblastic differentiation inside the cell simultaneously, resulting in an enhanced osteoblastic differentiation.

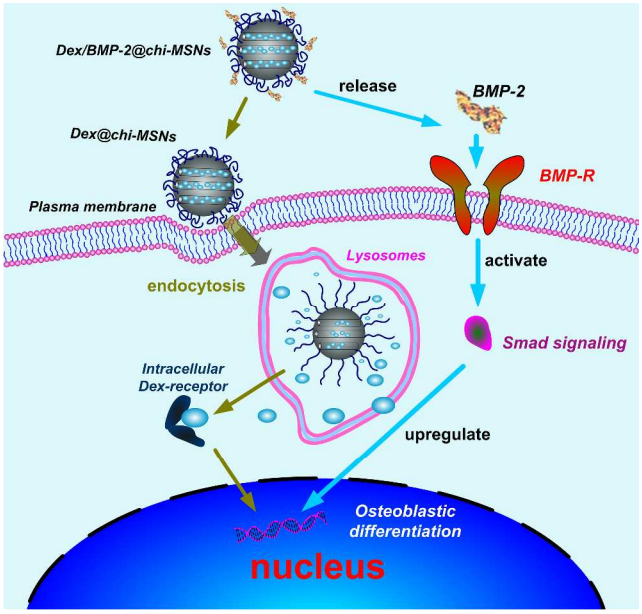

Fig. 9 Schematic diagram of Dex/BMP-2@chi-MSNs on osteoblast differentiation. (1) BMP-2 is quickly released and then activates the downstream Smad signaling by binding to specific cell surface BMP receptors. (2) Dex is delivered into cell by the endocytosed chi-MSNs and is released by pH-triggered chitosan changing in the lysosomes. Finally, BMP-2 and Dex induce and regulate osteoblast differentiation outside and inside the cell together, resulting in the enhnaced bone regeneration.

Conclusions

In this study, we have successfully synthesized a pH-responsive chitosan-functionalized MSNs dual-delivery system for targeted delivery of BMP-2 and Dex to enhance bone regeneration. The small Dex is loaded in the mesopores and the large BMP-2 is incorporated into the chitosan coating. The resulting chi-MSNs carrier demonstrates an enhanced co-loading capability of both BMP-2 and Dex, persistent bioactivity of BMP-2, and efficient intracellular and ensuing pH-responsive controlled release of Dex in cytosol. It shall be highlighted that the Dex/BMP-2@chi-MSNs dual-drug delivery system displays enhanced osteoblast differentiation of bMSCs cells *in vitro* and bone formation *in vivo*, which provides preclinical data for the potential applications of dual-delivery mode of drug/protein in promoting bone formation and bone defect repair.

Acknowledgements

The authors wish to express their gratitude to the financial supports from National Basic Research Program of China (973 Program, No. 2012CB933600), the 111 Project (B14018), National Natural Science Foundation of China (No.31100679 and No.31400817), Chinese Postdoctoral Science Foundation (2013M541484) and Shanghai Nanotechnology Special Foundation (No. 11nm0506300). This study was also supported by Program for New Century Excellent Talents in University (No NCET-11-0640) and the national Special Fund for State Key Laboratory of Bioreactor Engineering (No.2060204).

Notes and references

[a] *The State Key Laboratory of Bioreactor Engineering, East China University of Science and Technology, Shanghai 200237, PR China*

[b] *Key Laboratory for Ultrafine Materials of Ministry of Education, Engineering Research Center for Biomedical Materials of Ministry of Education, East China University of Science and Technology, Shanghai 200237, PR China. Fax:+86 21-64251358; Tel: +86 21-64251358; Email: yyuan@ecust.edu.cn; liucs@ecust.edu.cn*

[c] *State Key Laboratory of Chemical Engineering and Department of Chemistry, East China University of Science and Technology, Shanghai 200237, China*

† Electronic Supplementary Information (ESI) available: *In vitro* MTT and ALP activity results of MSNs and chi-MSNs, BMP-2 released from Dex/BMP-2@chi-MSNs and BMP-2@chi-MSNs at pH 6.0 and 7.4, Dex released from Dex@chi-MSNs and Dex/BMP-2@chi-MSNs at pH 6.0 and 7.4; N_2 adsorption/desorption isotherms and surface properties of chi-MSNs at pH 6.0 and 7.4, sense and antisense primers utilized for real-time PCR amplification, secondary structure of BMP-2 released from MSNs and chi-MSNs at pH 6.0 and 7.4 in PBS as determined by CD spectra. See DOI: 10.1039/b000000x/

1. G. Mundy, R. Garrett, S. Harris, J. Chan, D. Chen, G. Rossini, B. Boyce, M. Zhao and G. Gutierrez, *Science*, 1999, **286**, 1946-1949.
2. N. R. Jorgensen, Z. Henriksen, O. H. Sorensen and R. Civitelli, *Steroids*, 2004, **69**, 219-226.
3. C. Przybylowski, T. Quinn, A. Callahan, M. Kaplan, A. Golding, C. Alesi, M. Ammar, C. E. LeBlon, Y. Guo, X. H. Zhang and S. S. Jedlicka, *J. Mater. Chem.*, 2012, **22**, 10672-10683.
4. H. Kim, H. Suh, S. A. Jo, H. W. Kim, J. M. Lee, E. H. Kim, Y. Reinwald, S. H. Park, B. H. Min and I. Jo, *Biochem. Biophys. Res. Commun.*, 2005, **332**, 1053-1060.
5. E. Gazzerro and E. Canalis, *Rev. Endocr. Metab. Dis.*, 2006, **7**, 51-65.
6. Y. Mikami, K. Omoteyama, S. Kato and M. Takagi, *Biochem. Biophys. Res. Commun.*, 2007, **362**, 368-373.
7. Y. Su, Q. Q. Su, W. Liu, M. Lim, J. R. Venugopal, X. M. Mo, S. Ramakrishna, S. S. Al-Deyab and M. El-Newehy, *Acta Biomater.*, 2012, **8**, 763-771.
8. Y. Mikami, M. Asano, M. J. Honda and M. Takagi, *J. Cell. Physiol.*, 2010, **223**, 123-133.
9. M. Jager, J. Fischer, W. Dohrn, X. N. Li, D. C. Ayers, A. Czibere, W. C. Prall, S. Lensing-Hohn and R. Krauspe, *J. Orthop. Res.*, 2008, **26**, 1440-1448.
10. K. Kleinschmidt, F. Ploeger, J. Nickel, J. Glockenmeier, P. Kunz and W. Richter, *Biomaterials*, 2013, **34**, 5926-5936.
11. L. Y. Cao, J. Wang, J. Hou, W. L. Xing and C. S. Liu, *Biomaterials*, 2014, **35**, 684-698.
12. V. E. Santo, K. Sato, J. Ratanavaraporn, M. E. Gomes, J. F. Mano, R. L. Reis and Y. Tabata, *J. Tissue. Eng. Regen. Med.*, 2012, **6**, 330.
13. M. Everts, R. J. Kok, S. A. Asgeirsdottir, B. N. Melgert, T. J. M. Moolenaar, G. A. Koning, M. J. A. van Luyn, D. K. F. Meijer and G. Molema, *J. Immunol.*, 2002, **168**, 883-889.
14. J. M. Oliveira, R. A. Sousa, N. Kotobuki, M. Tadokoro, M. Hirose, J. F. Mano, R. L. Reis and H. Ohgushi, *Biomaterials*, 2009, **30**, 804-813.
15. X. Du, B. Y. Shi, J. Liang, J. X. Bi, S. Dai and S. Z. Qiao, *Adv. Mater.*, 2013, **25**, 5981-5985.
16. M. Chen, X. X. He, K. M. Wang, D. G. He, S. N. Yang, P. C. Qiu and S. Y. Chen, *J. Mater. Chem. B*, 2014, **2**, 428-436.
17. T. Chen, H. Yu, N. E. Yang, M. D. Wang, C. D. Ding and J. J. Fu, *J. Mater. Chem. B*, 2014, **2**, 4979-4982.
18. Y. X. Tang, Z. G. Teng, Y. Liu, Y. Tian, J. Sun, S. J. Wang, C. Y. Wang, J. D. Wang and G. M. Lu, *J. Mater. Chem. B*, 2014, **2**, 4356-4362.
19. Q. Gan, X. Y. Lu, W. J. Dong, Y. Yuan, J. C. Qian, Y. S. Li, J. L. Shi and C. S. Liu, *J. Mater. Chem.*, 2012, **22**, 15960-15968.
20. E. Aznar, M. D. Marcos, R. Martinez-Manez, F. Sancenon, J. Soto, P. Amoros and C. Guillem, *J. Am. Chem. Soc.*, 2009, **131**, 6833-6843.
21. Y. L. Zhao, Z. X. Li, S. Kabehie, Y. Y. Botros, J. F. Stoddart and J. I. Zink, *J. Am. Chem. Soc.*, 2010, **132**, 13016-13025.
22. J. Wu and M. Sailor, *Adv. Funct. Mater.*, 2009, **19**, 733-741.
23. A. Popat, J. Liu, G. Q. Lu and S. Z. Qiao, *J. Mater. Chem.*, 2012, **22**, 11173-11178.
24. H. J. Shen, H. Shi, M. Xie, K. Ma, B. Li, S. Shen, X. S. Wang and Y. Jin, *J. Mater. Chem. B*, 2013, **1**, 3906-3917.
25. Z. W. Deng, Z. P. Zhen, X. X. Hu, S. L. Wu, Z. S. Xu and P. K. Chu, *Biomaterials*, 2011, **32**, 4976-4986.
26. F. Chen and Y. C. Zhu, *Micropor. Mesopor. Mater.*, 2012, **150**, 83-89.
27. T. Y. Wu, Z. B. Zhou, Z. W. He, W. P. Ren, X. W. Yu and Y. Huang, *J. Biomed. Mater. Res. A*, 2014, **102**, 68-75.
28. L. Zhao, E. F. Burguera, H. H. K. Xu, N. Amin, H. Ryou and D. D. Arola, *Biomaterials*, 2010, **31**, 840-847.
29. I. Slowing, B. G. Trewyn and V. S. Y. Lin, *J. Am. Chem. Soc.*, 2006, **128**, 14792-14793.
30. K. A. Fisher, K. D. Huddersman and M. J. Taylor, *Chem. Eur. J.*, 2003, **9**, 5873-5878.
31. J. Zhang, H. J. Zhou, K. Yang, Y. Yuan and C. S. Liu, *Biomaterials*, 2013, **34**, 9381-9392.
32. Q. Gan, X. Y. Lu, Y. A. Yuan, J. C. Qian, H. J. Zhou, X. Lu, J. L. Shi and C. S. Liu, *Biomaterials*, 2011, **32**, 1932-1942.
33. G. Lawrie, I. Keen, B. Drew, A. Chandler-Temple, L. Rintoul, P. Fredericks and L. Grondahl, *Biomacromolecules*, 2007, **8**, 2533-2541.
34. F. Q. Tang, L. L. Li and D. Chen, *Adv. Mater.*, 2012, **24**, 1504-1534.
35. C. L. Dai, H. Guo, J. X. Lu, J. L. Shi, J. Wei and C. S. Liu, *Biomaterials*, 2011, **32**, 8506-8517.
36. Q. Gan, D. W. Dai, Y. Yuan, J. C. Qian, S. Sha, J. L. Shi and C. S. Liu, *Biomed. Microdevices*, 2012, **14**, 259-270.
37. P. Habibovic, T. M. Sees, M. A. van den Doel, C. A. van Blitterswijk and K. de Groot, *J. Biomed. Mater. Res. A*, 2006, **77A**, 747-762.
38. A. F. Oliveira, S. Gemming and G. Seifert, *J. Phys. Chem. B*, 2011, **115**, 1122-1130.
39. J. H. Park, C. E. Wasilewski, N. Almodovar, R. Olivares-Navarrete, B. D. Boyan, R. Tannenbaum and Z. Schwartz, *Biomaterials*, 2012, **33**, 7386-7393.
40. S. Santra, B. Liesenfeld, C. Bertolino, D. Dutta, Z. H. Cao, W. H. Tan, B. M. Moudgil and R. A. Mericle, *J. Lumin.*, 2006, **117**, 75-82.

A proton-triggered chitosan-functionalized MSNs ensemble is fabricated to enhance the cellular uptake of dexamethasone and maintain the osteoinductive activity of BMP-2. It can indeed enhance the synergistic effect of BMP-2 and dexamethasone in osteoblast differentiation *in vitro* and *in vivo*.